HHS Public Access

Author manuscript

Exp Neurol. Author manuscript; available in PMC 2022 January 01.

Published in final edited form as:

Exp Neurol. 2022 January ; 347: 113880. doi:10.1016/j.expneurol.2021.113880.

Mutation of the murine *Prickle1 (R104Q)* causes phenotypes analogous to human symptoms of epilepsy and autism

Yue Ban, **Ting Yu**, **Jingyi Wang**, **Xiaojia Wang**, **Can Liu**, **Clayton Baker**, **Yimin Zou***

Neurobiology Section, Biological Sciences Division, University of California, San Diego, La Jolla, CA 92093, United States of America

Abstract

Epilepsy and autism spectrum disorders (ASD) frequently show comorbidity, suggesting shared or overlapping neurobiological basis underlying these conditions. *R104Q* is the first mutation in the *PRICKLE 1(PK1)* gene that was discovered in human patients with progressive myoclonus epilepsy (PME). Subsequently, a number of mutations in the *PK1* gene were shown to be associated with either epilepsy, autism, or both, as well as other developmental disorders. Using CRISPR-Cas9-mediated gene editing, we generated a PK1^{R104Q} mouse line. The mutant mice showed reduced density of excitatory synapses in hippocampus and impaired interaction between PK1 and the repressor element 1(RE-1) silencing transcription factor (REST). They also displayed reduced seizure threshold, impaired social interaction, and cognitive functions. Taken together, the PK1^{R104Q} mice display characteristic behavioral features similar to the key symptoms of epilepsy and ASD, providing a useful model for studying the molecular and neural circuit mechanisms underlying the comorbidity of epilepsy and ASD.

Keywords

Prickle1; Prickle1 R104Q; Mouse model; Seizure threshold (PTZ); Three-chamber social interaction assay; Barnes maze; Novel object recognition; Planar cell polarity; REST

1. Introduction

Epilepsy and ASD are common neurodevelopmental disorders affecting approximate 0.6% and 1.8% of children in the U.S, respectively (Maenner et al., 2020; Russ et al., 2012). Epilepsy is characterized by recurring seizures. ASD is diagnosed based on behavioral symptoms including deficits in social function and communication, intellectual disability and stereotypical repetitive behaviors. Epilepsy and ASD are frequently comorbid. Epilepsy occurs in 6–27% of human patients with ASD, while 5–37% of epileptic patients show

*Corresponding author: yzou@ucsd.edu (Y. Zou).

Credit author statement

Y.Z., Y.B. and T.Y. designed the experiments; Y.B, T.Y., J.W., X.W., C. L., and C.B. performed all experiments under the supervision of Y.Z; Y.B, T.Y., J.W., X.W., C.L.,C.B., and Y.Z. analyzed and interpreted data; Y.B. and Y.Z. wrote the paper; and all authors read and commented on the manuscript.

Declaration of Competing Interest

Y.Z. is the founder of VersaPeutics and has equity, compensation and interim managerial role. The terms of this arrangement have been reviewed and approved by the University of California, San Diego in accordance with its conflict-of-interest policies.

ASD symptoms. And the prevalence of epilepsy accompanied ASD is greatest among patients with intellectual disability (Jeste and Tuchman, 2015). The underlying pathological mechanisms of both disorders remain to be elucidated. However, the high comorbidity of these disorders suggests shared or overlapping neurobiological basis.

The homozygous recessive mutation *R104Q* in the *PK1* gene was first discovered in three consanguineous families with myoclonus epilepsy (Bassuk et al., 2008). Subsequent studies have reported more heterozygous and homozygous *PK1* mutations in human patients with epilepsy (*R84Q*, *R144H*, *Y472H*, and *A274T*) or epilepsy accompanied with ASD (D482N) (Algahtani et al., 2019; Mastrangelo et al., 2018; Tao et al., 2011; Todd and Bassuk, 2018). Moreover, mutations in the *PK1* gene could lead to epilepsy- and ASD-related phenotypes across a variety of species (Bassuk et al., 2008; Paemka et al., 2013; Tao et al., 2011). Defects in nervous system development, particularly those affecting synaptic functions, are thought to contribute to epilepsy and ASD (Bozzi et al., 2018). PK1 is a core component of the planar cell polarity (PCP) signaling. Recent studies showed that components of the PCP signaling pathway are major regulators of glutamatergic synapse formation and maintenance (Ban et al., 2021, In Press Science Advances) (Feng et al., 2021; Thakar et al., 2017; Zou, 2020). Therefore, *PK1* mutations may affect PCP functions in neural circuit development, including synapse formation. Mouse *PK1* is abundantly expressed in many regions of the central nervous system (Lein et al., 2007). It encodes a protein consisting of a N-terminal PET (Prickle, Espinas, Testin) domain and three C-terminal LIM (Linl-1, Isl-1, Mec-3) domains. Previous in vitro studies suggest that PK1 interacts with REST and might serve as a nuclear receptor for REST (Shimojo and Hersh, 2003, 2006). Therefore, PK1 may also have functions in addition to being a core component of the PCP signaling pathway.

In this study, we used CRISPR-Cas9-mediated gene editing to generate mice carrying the *R104Q* mutation, which was the first identified *PK1* mutation and is associated with PME. At the cellular and molecular level, these mutant mice had reduced density of excitatory synapses and impaired binding between PK1 and REST. At the behavioral level, mutant mice displayed lower seizure threshold, impaired social interaction as well as mild intellectual disability. Taken together, our $PK1^{R104Q}$ mice may provide a mouse model for studying the underlying pathophysiological mechanisms of epilepsy-ASD comorbidity.

2. Materials and methods

2.1. Generation of the PK1 R104Q mice

The *PK1* guide RNAs (gRNAs) were designed using the online CRISPR tool (http://tools.genome-engineering.org) and tested in the N2A cell line before injections. The embryo microinjection was carried out at the UCSD transgenic core. The CRISPR mix containing Cas9 protein, sgRNA, and the single-stranded oligodeoxynucleotides (ssODN) repair template was delivered by pronuclear injection into 0.5-day-old C57BL6 embryos. On the same day, injected embryos were implanted into the fallopian tube of recipient ICR females. Pups were born 21 days post implantation and genotyped. To avoid potential off-target effects, we backcrossed the mutant mice to the B6 background for seven generations before conducting analyses. The sgRNA sequence used for generating this mouse line is TCAAACTCTTGTCCAGAGCT. Sequence of the ssODN is

TTTGAGCGAAGAAGAGAAGAAGGAGCTGCAGGTGTTCAGTGCTCAGCAAAAGAA AGAAGCTCTGGGGAGAGGAACTATTAAGTTGTTGTCCAGAGCTGTGATGCACGCC GTGTGTGAGCAGGTAGGCCCTCTCTAGAGCGAGCAGAGGGTTGGTGGGAGC.

2.2. Genotyping

Genotyping of all animals was done by PCR using genomic DNA prepared from tails. Tail lysates were prepared by immersing 0.5-cm tail pieces in 300 μl 50 mM NaOH solution, and incubating for 1 h at 95°C to lyse the tissue. Tail lysates were mixed with 30 ul 1 M Tris (pH 8) by vortexing and then centrifuged at 12000 *xg* for 2 min. The supernatants were used as DNA templates for PCR (Apex Taq RED 2× Master Mix, Genesee Scientific, 42138). WT allele was genotyped using primers: 5′-TGGGGAGAGGAACCATCAAACTC-3′ and 5′- ACCGAGGCTTGAGCAGTTCAG-3′. The PK1 R104Q mutant allele was genotyped using primers: 5′- CTGGGGAGAGGAACTATTAAGTTG-3′ and 5′- ACCGAGGCTTGAGCAGTTCAG-3′. The PCR products for WT and mutant alleles are 717 bp and 718 bp respectively.

2.3. Immunohistochemistry

Immunohistochemistry was performed as previously described (Thakar et al., 2017). Briefly, mice were first perfused with phosphate buffered saline (PBS) and subsequently with 4% paraformaldehyde (PFA) dissolved in PBS. Brains were dissected out and fixed in 4% PFA in PBS overnight at 4°C. Brains were cryoprotected by immersing in 30% sucrose until the tissue sank to the bottom and then embedded in OCT (Sakura, 25608–930)/ 30% sucrose (1:1) mixture and frozen on dry ice. 40 μm-thick coronal free-floating sections were collected, treated with 1% SDS for antigen retrieval, and stained with antibodies against Bassoon (Synaptic Systems, 141004) and PSD-95 (Abcam, ab12093). Fluorescent image stacks (20 images per stack) were acquired using LSM510 or LSM 880 Zeiss confocal microscopes with a 63× oil-immersion lens and 2.5× zoom. Quantification and colocalization analyses of synaptic puncta were performed using the ImageJ' plugin, "synapse counter"(Dzyubenko et al., 2016). Investigators were blinded to the genotypes of animals while conducting imaging and analysis.

2.4. Immunoprecipitation (IP) and western blot

Nuclear and cytoplasmic lysates from adult mouse hippocampus (HPC) were prepared using NE-PER™ Nuclear and Cytoplasmic Extraction Reagents (ThermoFisher Scientific, 78833). Lysates were IPed with anti-REST antibody (Abcam, ab202962, lot#GR3259950–9)) and with Dynabeads® Protein G (ThermoFisher Scientific, 10007D). Rabbit IgG (Millipore Sigma, 12–370, lot#3281600) was used as a negative control. Denatured protein samples were run in an 8% SDS-PAGE gel (home-made). Proteins were then transferred onto a Immobilon-P PVDF membrane (Millipore Sigma; IPVH00010), blocked with 5% non-fat dry milk in TBST (0.05% Tween-20 in Tris-buffered saline), and incubated with primary antibodies diluted in blocking buffer overnight at 4°C. Membrane was washed three times in TBST for 10 min each and incubated with secondary antibodies for 1 h at room temperature followed by the same washing steps. Bands were detected by incubating the membrane with WestPico chemiluminescent substrate (ThermoFisher Scientific, 34580) and documented with X-ray film (ThermoFisher Scientific, 34091). Primary antibodies used for western

blot include anti-PK1 (Proteintech, 22589–1-AP, lot#00018803), anti-PK2 (Millipore Sigma, MABN1529, lot#Q2785035), anti-HSP90 beta (ThermoFisher Scientific, PA3–012, lot#TH269376), anti-HDAC1 (ThermoFisher Scientific, PA1–860, lot#UH292524), and anti-GAPDH (Millipore Sigma, MAB374, lot#3291346).

2.5. Overview of mouse behavioral assays

PK1$^{R104Q/+}$ mice were backcrossed into wildtype (WT) C57BL/6 for seven generations. All behavioral tests were performed with mice 2 to 3 months of age. Mice were weaned at P21 and housed in groups of two to five of the same gender. They were maintained under a 12-h light/dark cycle with ad libitum access to food and water, except during the tests. One cohort of mice ran through a behavioral test battery designed to assess locomotor activity, exploratory activity, anxiety-like behavior, and cognitive phenotypes. Tests were run in the order listed: open field test (day1), elevated plus maze (day2), light-dark transition (day3), novel object recognition (day4–5), three-chamber social interaction (day8–10), and Barnes maze (day17–26) (Bailey and Crawley, 2009; Crawley and Paylor, 1997; Janecka et al., 2017; Lad et al., 2010; McIlwain et al., 2001; Paylor et al., 2006). The housing room for mice used in the test battery was maintained on a reversed 12-h light/12-h dark cycle with white lights on from 8 pm to 8 am. Tests in battery were performed in the dark cycle between 10 am and 4 pm. Activities of mice in the test battery were captured using the EverFocus® 1080P camera mounted on the ceiling above the apparatus and streamed to the image acquisition software IC Capture (The Imaging Source). Videos were analyzed using the software Viewer (Biobserve). PTZ injection was performed using a different cohort of mice without training history, which were housed in normal light-dark cycle with white lights on from 7 am to 7 pm. PTZ injection experiments were conducted in the light cycle between 9 am to 3 pm. Both male and female mice were used in these assays. We pooled data from male and female animals together since we did not detect differences in their performance based on sex. On the test day, mice were habituated to the behavior room for 1 h before testing began. All apparatuses were cleaned with 70% (*v*/v) ethanol between animals. Visual cues were minimized unless they were required. Littermate controls were used in all tests. Investigators who performed the behavioral tests and video analysis were blind to the genotypes of tested animals.

2.5.1. Open field test—The open field arena (40 × 40 × 34 cm^3) is made of non-reflective gray plastic. Each mouse was placed in the arena facing the walls of the releasing corner (same location for all tested mice). Mice were allowed to freely explore the arena for 10 min. Experiments were conducted under dim red light. For analysis, the open field arena was divided into a 20 cm × 20 cm central zone and the surrounding border zone. The center of the mouse's body was tracked. Total distance and time spent in the border zone was measured. Thigmotaxis (a tendency to remain close to the vertical wall) was calculated as the proportion of time animals stay in the border zone.

2.5.2. Light dark transition test—The light dark box (40 × 40 × 34 cm^3; Stoelting) is composed of a dark compartment and a light compartment of equal size, separated by a partition with a door. The dark compartment was painted black with a closed top, whereas the light compartment was painted white with an open top and brightly illuminated (600 lx)

with an indirect light source. The door connecting the two compartments was blocked until the animal was released to the center of the light chamber. Individual mouse was allowed to move freely between the two compartments for 10 min. For analysis, the center of the body was tracked when animals explored the light compartment. The number of total transitions and the time spent in the light chamber was measured.

2.5.3. Elevated plus maze—The elevated plus maze (Stoelting) is made of non-reflective gray plastic and consists of four arms (15 cm long and 5 cm wide). Two open arms (without wall) and two closed arms (enclosed by 15 cm high walls) are connected to a central platform (5 cm × 5 cm). Each arm is attached to a sturdy metal leg to raise the apparatus 50 cm from the ground. Experiments were conducted in a brightly-lit area. Each mouse was placed in the central platform facing one of the closed arms and allowed to freely explore the maze for 10 min. For analysis, the entry in any arm was counted when all four paws were located within the space of the arm. Time spent in the open arms were measured. Animals fell off the maze were excluded from analysis.

2.5.4. Novel object recognition test—The test was conducted in a customized arena which is 40 cm long, 25 cm wide, and 34 cm high. Individual animals were habituated to the empty arena for 30 min 24 h before the training session. During the training session, two identical objects were placed in opposite directions ~8 cm away from the corner in order to distinguish between the animal's preferences to the corner or the objects. Objects were customized geometric solids with different shapes and textures. Objects were secured to the arena with sticky magnets to prevent mice from moving them. Mice were placed in the center of the arena and allowed to explore freely for 5 min. 24 h later, animals' recognition memory was tested by swapping one of the familiar objects with a novel object. The test was performed under dim red light during the dark phase of the cycle. The snout of each mouse was tracked and interaction time was measured as time spent with snouts within 2 cm around the object. Animals spending less than 20 s exploring the two objects were excluded from analysis.

2.5.5. Three chamber social approach test—The social approach apparatus is a rectangular non-transparent three-chambered plexiglass box. Each chamber is 40 cm long, 20 cm wide, and 20 cm high. Dividing walls are made from clear plexiglass with small openings (10 cm wide and 8 cm high) which can be blocked by sliding doors. In the first 10-min session, mice were habituated to the center chamber with the two openings blocked. Immediately after the first session was finished, the two sliding doors were removed to allow animals to explore the three chambers freely for 10 min. Before the test session, two steel wire pencil cups were placed in each of the side chambers. An age and gender-matched stranger mouse was placed under one of the inverted cups. The location of the stranger mouse was randomly arranged for each tested animal. Stranger mice were habituated to the inverted wire cup and the Plexiglass chamber prior to the experiments. Each stranger mouse was placed under a clean wire cup in one of the two side chambers for 10 min, and this was repeated for three times. Animals showing signs of aggression and disruptive behaviors, such as continuous bar-biting were not used in the test. During the test session, an individual mouse was placed in the center chamber and allowed to explore the three chambers freely

for 10 min. 1 h later, social memory was tested by placing a novel mouse underneath the wire cup located in the empty chamber and measuring the animal's preference between the familiar mouse and the novel mouse. The test was performed under dim red light during the dark phase of the cycle. The snouts of the mice were tracked and interaction time was measured as time spent with snouts within 2 cm surrounding the wire cup. Experiments in which the stranger mouse showed signs of aggression and disruptive behaviors were excluded from analysis.

2.5.6. Barnes maze test—The Barnes maze apparatus is a customized white circular plexiglass table (90 cm diameter) with twenty circular holes (5 cm diameter) located equidistantly from the perimeter. The maze was elevated 56 cm above the ground. Four colored geometric shapes (cone, cross, triangle and circle) equally spaced around the table were used as extra-maze visual cues. The escape box is a black Plexiglas box (15 × 6 × 6.6 cm^3) with a ramp covered with black plastic mesh which allows the animal to easily enter the escape box. Ceiling lights were positioned 192 cm above the maze (~800 lx) and a buzzer (2 kHz, 90 dB) were used as aversive stimuli.

The Barnes maze task was run over the course of 11 days in 4 phases: habituation (day0), acquisition training (day1-day4), probe test (day5), and reversal training (day6-day9). On the habituation day, each animal was placed in the maze next to a hole with escape box, restrained underneath a clear 2 litter glass beaker and given 5 min to enter the escape box through the hole. If they did not enter on their own, they were guided by the experimenter to enter the escape box and allowed to stay in the escape box for 1 min before being returned to its home cage. The habituation procedure allowed animals to experience the aversive bright light and to practice using the ramp to step down to the escape box.

During the acquisition training phase, only the target hole had the escape box underneath, the other 19 holes had "false escapes boxes" (a shallow black box which is 5 cm long, 5 cm wide and 1.5 cm deep) attached underneath. Locations of target hole were randomly arranged for each animal and covered all the four quadrants of the maze. An individual mouse was placed underneath a start chamber (a black cardboard box) located in the center of the maze for 15 s allowing the animal to face a random direction. A buzzer was turned on and the start chamber was removed to start the trial. If a mouse successfully entered the escape box, the buzzer was turned off and the trial ended. The mouse was allowed to stay in the escapes box for 1 min before being returned to its home cage. Mice failing to enter the escape box during the 3 min session were guided into the escape box by the investigator. Animals were trained twice a day with 15 min inter-trial interval for 4 days. Location of the target hole was kept constant during the training phase and was randomly selected for each animal. The latency to locate the target hole was measured. If mice failed to enter the escape box within the 3 min training session, latency was counted as 3 min.

For the probe test on day 5, the escape box was removed and all of the twenty holes led to false escape boxes. A mouse was released from the start chamber and allowed to freely explore the maze for 3 min with the buzzer turned on. The center of the body was tracked and the time animals spent in each quadrant was measured. Procedures of the reversal training were similar to the acquisition training phase, except that the location of the target

hole was opposite to its location during the acquisition training phase. Animals fell off the maze were excluded from analysis.

2.5.7. PTZ injection to induce seizure—2 mg/ml PTZ (Sigma-Aldrich, P6500) was prepared in sterile 0.9% (*w/v*) NaCl. 50 mg/kg PTZ was injected intraperitoneally with a 1-ml syringe attached to a 27-gauge needle into left or right quadrant of the abdomen of each mouse. An individual animal was placed in a clear plastic cage with bedding and monitored by a side view webcam for 30 min. The latencies to the first jerk and tonic-clonic seizure were recorded by observer.

2.6. Statistical analysis

Methods and complete results of statistical analysis were described in corresponding figure legends. All statistical analysis was performed using the software GraphPad Prism.

3. Results

3.1. Reduced density of glutamatergic synapses in the hippocampus of PK1 R104Q mice

PK1 is a core component of the PCP signaling pathway, which was found to be critical for the assembly and maintenance of glutamatergic synapses (Ban et al., 2021, In Press Science Advances) (Feng et al., 2021; Thakar et al., 2017; Zou, 2020). PK1 is highly expressed in mouse HPC, where it localizes to both the cell nucleus and the postsynaptic density (PSD) of neurons (Ban et al., 2021, In Press Science Advances). We used CRISPR-Cas9 to generate a *PK1 R104Q* knock-in mice (Fig. 1A–C). To avoid potential off-target effects, we backcrossed the *PK1 R104Q* knock-in mice to WT B6 background for seven generations before we systematically analyzed and quantified phenotypes. To determine whether the *PK1 R104Q* mutation affects protein expression, the synaptosome fraction was harvested from the cortex and HPC of P14 mice for Western blot analysis. We did not detect significant changes in the protein level of PK1 between *WT* and mutant *PK1* mice, suggesting *PK1 R104Q* mutation does not affect the stability of PK1 protein (Fig. 1D and E). To assess the effects of *PK1 R104Q* on the formation of excitatory synapses, we performed immunohistochemistry at P14 and adult mice (2-month old) to examine synaptic density in the stratum radiatum in the CA1 region of the HPC, where Schaffer collateral fibers of CA3 pyramidal neurons form glutamatergic synapses on the dendrites of CA1 pyramidal neurons (Fig. 2A). Excitatory synapses were identified as colocalized puncta of the presynaptic marker Bassoon and the postsynaptic marker PSD-95. We observed a significant 20% reduction in the number of PSD-95-positive excitatory synapses in $PK1^{R104Q/R104Q}$ mice at P14 and 35% reduction in adult heterozygous and homozygous mutant mice (Fig. 2B–D). These results suggest that PK1 plays a role in the assembly and maintenance of the PSD-95-positive excitatory synapses and that the *R104Q* mutation impairs its role in synapse formation and maintenance.

3.2. PK1 R104Q mutation impaired its interaction with REST in vivo

The *R104Q* mutation of *PK1* lies within the highly conserved PET domain of the PK1 protein, which mediates protein-protein interactions and is engaged in PK1 membrane insertion (Sweede et al., 2008; Tree et al., 2002). Previous in vitro studies suggest that PK1

interacts with REST and may serve as a nuclear receptor for REST (Shimojo and Hersh, 2003, 2006). During mouse embryogenesis, REST is restrictedly expressed in nonneuronal cells to silence neuronal gene expression resulting in the restriction of membrane excitability characteristics to neurons (Chong et al., 1995). In later stages of development, REST also modulates gene expression in neurons. It may serve as either a repressor or an activator, depending on the spatial and temporal context of its expression (Ballas et al., 2005; Lu et al., 2014). The *R104Q* mutation of human PK1 protein decreases its interaction with REST in in vitro assays using HEK cells (Bassuk et al., 2008). Here, we asked whether REST interacts with PK1 and whether the *R104Q* mutation impairs their interaction in vivo. We first biochemically fractionated the mouse HPC into the cytoplasmic and nuclear fraction (Fig. 2E) and found both PK1 and REST were localized in both the cytoplasm and nucleus. REST was more abundant in the nuclear fraction, whereas, PK1 was enriched in the cytoplasm (Fig. 2F). The cytoplasmic and nuclear lysates were then used for coIP with the anti-REST antibody. Endogenous REST was found to interact with PK1 but not PK2 in both the cytoplasm and nucleus (Fig. 2F). To test whether *R104Q* mutation impairs REST's interaction with PK1, we performed coIP and western blot using HPC nuclear extracts of $PK1^{R104Q/R104Q}$ mice and their *WT* littermates. We found less PK1 was coIPed with endogenous REST from HPC nuclear extracts of $PK1^{R104Q/R104Q}$ mice (Fig. 2G and H). Therefore, *PK1 R104Q* mutation impaired its interaction with REST in vivo.

3.3. Decreased seizure threshold in the PK1 R104Q heterozygous mice

The *PK1 R104Q* homozygous mutation was first found in three consanguineous families with myoclonic epilepsy (Bassuk et al., 2008). To determine whether the *R104Q* point mutation in *PK1* may cause epileptic seizures in mice, we tested seizure threshold using the $GABA_A$ receptor antagonist Pentylenetetrazole (PTZ). Following a single administration of 50 mg/kg PTZ, the latencies to myoclonic jerk and tonic-clonic seizure were measured. All animals tested showed myoclonic jerk and no statistically significant difference was detected in the latency among the three groups of animals (Fig. 2I). However, $PK1^{R104Q/+}$ mice showed significantly shorter latencies to tonic-clonic seizure than mutant homozygous and *WT* littermates (Fig. 2J). While humans with *PK1 R104Q* homozygous mutations show myoclonic epilepsy, we found heterozygous *R104Q* mutation enhanced seizure susceptibility more than homozygous *R104Q* in mice.

3.4. Impaired social approach in the PK1 R104Q mutant mice

PK1 mutations in humans were found to be associated with both myoclonic epilepsy and ASD (Todd and Bassuk, 2018). $PK1^{+/-}$ mice exhibited abnormal social interactions consistent with ASD-like behavior (Paemka et al., 2013). To assess the social motivation of *PK1 R104Q* mice, we used the three-chamber social interaction task to analyze social approach, in which the preference of a subject mouse for a wire cup containing a stranger mouse versus an empty wire cup was examined (Fig. 3A). As expected, *WT* littermates showed a strong preference for the cup containing a mouse, whereas, *PK1 R104Q* mutant mice displayed profound deficit in social approach behavior (Fig. 3B and C). In contrast to the deficits in sociability, *PK1 R104Q* heterozygous and homozygous mice displayed normal social recognition memory as determined by a three-chamber social novelty task. In this test, social recognition was determined by the increased time that a subject mouse spent

interacting with a novel mouse compared to the time it spent interacting with a familiar mouse (Fig. 3A). All mice spent significantly more time exploring the novel mouse than the familiar mouse (Fig. 3B and D).

3.5. PK1 R104Q mutation does not affect anxiety level

One possible explanation for the decreased time spent engaging in social behavior shown by *PK1 R104Q* mice is an increased anxiety level. Therefore, we used several unconditioned laboratory tests to examine whether *PK1 R104Q* affects animals' anxiety levels, the open field arena (OFA), elevated plus maze (EPM) and light-dark transition (LDT) tasks (Bailey and Crawley, 2009; Kulesskaya and Voikar, 2014; Prut and Belzung, 2003; Walf and Frye, 2007). A rodent with increased anxiety tends to spend less time exploring the unprotected and brightly lit space (e.g. the center area of the OF, the open arm of the EPM and the light chamber of the LDT apparatus). We found that the *PK1 R104Q* mutant mice did not show altered anxiety level (Fig. 4). In the OFA, mice in all groups showed similar overall exploratory activity determined by the total distance traveled (Fig. 4A). Anxiety level was evaluated by thigmotaxis, which is quantified by the proportion of time the animal stays at the periphery of the OFA, and no significant difference was observed among the three groups(Fig. 4B). In the LDT task, all tested mice showed similar general locomotor activity level assessed by the total number of transitions(Fig. 4C). *PK1 R104Q* mutation did not affect anxiety-related behavior in the LDT apparatus as all tested mice spent a similar amount of time in the light chamber(Fig. 4D). Finally, *PK1 R104Q* mutant animals spent a similar amount of time exploring the open arms of EPM compared with *WT* littermates(Fig. 4E), further confirming *PK1 R104Q* does not alter the animal's anxiety behavior in laboratory-built novel, unprotected and brightly lit areas.

3.6. Spatial memory deficit in PK1 R104Q heterozygous mice and novel object recognition deficit in PK1 R104Q homozygous mice

We then tested whether the *R104Q* mutation affected cognitive functions in mice. First used the Barnes maze task to examine the spatial navigational learning and memory. During the acquisition training phase, all tested mice displayed similar learning abilities(Fig. 5A). In the probe test to examine their spatial memory, unlike $PK1^{R104Q/R104Q}$ and *WT* mice, which spent significantly greater time in the target quadrant than the average time of other quadrants, $PK1^{R104Q/+}$ mice spent similar time in the target quadrant and other quadrants (Fig. 5B). To test whether the *PK1 R104Q* mice display difficulties in changing a learned pattern, we included a reversal training phase in the Barnes maze task. *PK1* mutant mice showed a similar degree of flexibility as their *WT* littermates(Fig. 5C). These results suggest that the heterozygous mutant mice, $PK1^{R104Q/+}$, but not the homozygous mutant mice display a mild deficit in spatial memory. Second, we performed novel objection recognition task (Fig. 5D). During the training phase, mice in the three groups spent similar amount of time exploring the two identical objects indicating no side preference(Fig. 5E–G). The total interaction time showed a trend of increase in the *PK1 R104Q* animals, but the difference is not statistically significant (Fig. 5H). During the novel object recognition phase, *WT* and *PK1 R104Q* heterozygous mutant mice displayed profound discrimination between the novel and familiar objects (Fig. 5I and J). Whereas, $PK1^{R104Q/R104Q}$ mice did not display strong preference to the novel object as shown by the significantly lower

discrimination index (Fig. 5I and J). The total time of object sniffing is similar among all groups during the object recognition phase (Fig. 5K). Together, these data suggest the *R104Q* mutation of *PK1* impaired the "no-matching-to-sample" memory (novel object recognition). The heterozygous mutation ($PK1^{R104Q/+}$) causes spatial memory deficit (in Barne's maze) not the homozygous mutation ($PK1^{R104Q/R104Q}$), whereas the homozygous mutation ($PK1^{R104Q/R104Q}$) causes impaired novel object recognition not the heterozygous mutation ($PK1^{R104Q/+}$).

4. Discussion

Epilepsy and ASD have significant comorbidity, suggesting that there are shared neurobiological mechanisms underlying these two disorders. Multiple *PK1* and *PK2* mutations in humans show either epilepsy or autism or both. But the logic of which mutations of which *PK* cause which disease has not been clear. Testing these mutations in mice may shed light on the role of PKs in normal synapse formation and function as well as shared molecular and circuit mechanisms of epilepsy and ASD. The *PK1 R104Q* mutation in humans causes PME not autism. However, the *PK1 D482N* mutation was implicated as a causative factor of ASD (Todd and Bassuk, 2018). Behavioral studies of $PK1^{+/-}$ mice revealed abnormal social behavior and repetitive behaviors (Paemka et al., 2013). Therefore, PK1 is a great candidate for studying comorbidity of epilepsy and ASD. Here, we made the *PK1 R104Q* knock-in mouse and found that it displayed characteristic behavioral phenotypes mimicking some of the key symptoms of both epilepsy and ASD, making this mouse an appealing tool. In addition, we also observed interesting differences between mouse and human. First, homozygous *PK1 R104Q* mutation causes myoclonus epilepsy in humans, whereas increased susceptibility to seizure was observed in mice carrying heterozygous *PK1 R104Q* mutation but not in homozygotes. In addition to seizure threshold, social interaction and spatial memory were also found to be impacted in heterozygous *PK1 R104Q* mutation; Second, although *PK1 R104Q* did not cause obvious ASD symptoms in humans, we observed social interaction deficits in both heterozygous and homozygous *PK1 R104Q* mutant mice. These interesting species differences may provide additional opportunities for us to understand the complex molecular and circuit mechanisms leading to epilepsy and ASD.

We made an interesting observation that the *PK1 R104Q* heterozygotes show lower seizure threshold, social interaction deficit and impaired spatial memory. The homozygotes show social interaction deficit and impaired novel object recognition. We propose that this may be caused by two PK1 functions which are potentially affected by the *R104Q* mutation. *PK1 R104Q* mutation causes the reduction of PK1-REST interaction and probably alters network activity patterns, including excitation/inhibition balance, as we observed reduced seizure threshold in heterozygotes. *PK1 R104Q* mutation may also affect PK1's role in synapse function or formation. In heterozygotes, there is one copy of WT *PK1*. In homozygotes, there is a complete lack of WT PK1 protein, potentially causing greater impact on the normal function or formation of synapses. We hypothesize that the network hyperactivity, commonly seen in seizures, may be somewhat cancelled in homozygotes because the synapses made by the mutant PK1 protein are not functional, resulting in a less severe phenotype in seizure threshold. Similarly, spatial memory may be impaired in heterozygotes

due to hyperactivity but not in homozygotes. We hypothesize that object recognition requires certain functions of PK1 in synapses, which are lost in the *PK1 R104Q* mutation. And that PK1 function is still present in *PK1 R104Q* heterozygotes but completely lacking in homozygotes. The hyperactivity in *PK1 R104Q* heterozygotes somehow does not affect object recognition or does not occur in the area/network required for object recognition.

It is interesting that *PK1 R104Q* mutation resulted in fewer excitatory synapses but lower seizure threshold. Indeed, both increase and decrease of excitation/inhibition ratio have been implicated in dysfunction of neuronal networks and behavioral deficits, due to the complexity of connectivity and cell types as well as homeostatic compensation of the networks (Nelson and Valakh, 2015). Future studies will be needed to sort out whether it is the loss of REST, which affects the overall neuronal excitability, or whether *PK1 R104Q* causes loss of excitatory synapses more on interneurons than on excitatory neurons and leads to lower seizure threshold and autism-like phenotypes.

In mammals, PK2 shares similar domain structures of PK1, and is also broadly expressed in multiple brain regions (Lein et al., 2007). Disrupted PK2 function led to autistic and epileptic phenotypes in both human and animal models (Sowers et al., 2013; Tao et al., 2011), further emphasizing the importance of PK-mediated signaling in the pathogenesis of epilepsy and ASD. Further analyses of the role and mechanisms of PK1 and PK2 in synapse formation, maintenance and plasticity will deepen our understanding of the molecular and cellular basis of these disorders, which will lead to the development of innovative diagnostic tools and therapeutic strategies.

Acknowledgments

We would like to thank members of the Zou lab for critical reading and comments on the manuscript. We thank the University of California San Diego (UCSD) Transgenic core for injecting sgRNA/Cas9 mRNA to make the PK1 R104Q mice. We thank Akum Grewal and Sogoli Sadraeinouri for mouse colony maintenance and genotyping. LSM880 Zeiss confocal microscopy imaging was performed at UCSD School of Medicine Light Microscopy Facility (Grant P30 NS047101). The graphical summary was created with BioRender.

Funding

This work was supported by RO1 MH116667 and R21 NS111648 to Y. Z.

Abbreviations:

ASD	autism spectrum disorders
PK	Prickle
REST	repressor element 1 silencing transcription factor
PCP	planar cell polarity
ssODN	single-stranded oligodeoxynucleotides
HPC	hippocampus
PTZ	pentylenetetrazole

PME	progressive myoclonus epilepsy
OFA	open field arena
LDT	light-dark transition
EPM	elevated plus maze
coIP	coimmunoprecipitation
WT	wildtype

References

Algahtani H, Al-Hakami F, Al-Shehri M, Shirah B, Al-Qahtani MH, Abdulkareem AA, Naseer MI, 2019. A very rare form of autosomal dominant progressive myoclonus epilepsy caused by a novel variant in the PRICKLE1 gene. Seizure 69, 133–139. [PubMed: 31035234]

Bailey KR, Crawley JN, 2009. Anxiety-Related Behaviors in Mice

Ballas N, Grunseich C, Lu DD, Speh JC, Mandel G, 2005. REST and its corepressors mediate plasticity of neuronal gene chromatin throughout neurogenesis. Cell 121, 645–657. [PubMed: 15907476]

Bassuk AG, Wallace RH, Buhr A, Buller AR, Afawi Z, Shimojo M, Miyata S, Chen S, Gonzalez-Alegre P, Griesbach HL, et al. , 2008. A homozygous mutation in human PRICKLE1 causes an autosomal-recessive progressive myoclonus epilepsy-ataxia syndrome. Am. J. Hum. Genet 83, 572–581. [PubMed: 18976727]

Ban, 2021. Sci. Adv 7 eabh2974 6 October 2021.

Bozzi Y, Provenzano G, Casarosa S, 2018. Neurobiological bases of autism-epilepsy comorbidity: a focus on excitation/inhibition imbalance. Eur. J. Neurosci 47, 534–548. [PubMed: 28452083]

Chong JA, Tapia-Ramírez J, Kim S, Toledo-Aral JJ, Zheng Y, Boutros MC, Altshuller YM, Frohman MA, Kraner SD, Mandel G, 1995. REST: a mammalian silencer protein that restricts sodium channel gene expression to neurons. Cell 80, 949–957. [PubMed: 7697725]

Crawley JN, Paylor R, 1997. A proposed test battery and constellations of specific behavioral paradigms to investigate the behavioral phenotypes of transgenic and knockout mice. Horm. Behav 31, 197–211. [PubMed: 9213134]

Dzyubenko E, Rozenberg A, Hermann DM, Faissner A, 2016. Colocalization of synapse marker proteins evaluated by STED-microscopy reveals patterns of neuronal synapse distribution in vitro. J. Neurosci. Methods 273, 149–159. [PubMed: 27615741]

Feng B, Freitas AE, Gorodetski L, Wang J, Tian R, Lee YR, Grewal AS, Zou Y, 2021. Planar cell polarity signaling components are a direct target of beta-amyloid-associated degeneration of glutamatergic synapses. Sci. Adv 7.

Janecka M, Marzi SJ, Parsons MJ, Liu L, Paya-Cano JL, Smith RG, Fernandes C, Schalkwyk LC, 2017. Genetic polymorphisms and their association with brain and behavioural measures in heterogeneous stock mice. Sci. Rep 7, 41204. [PubMed: 28145470]

Jeste SS, Tuchman R, 2015. Autism spectrum disorder and epilepsy: two sides of the same coin? J. Child Neurol 30, 1963–1971. [PubMed: 26374786]

Kulesskaya N, Voikar V, 2014. Assessment of mouse anxiety-like behavior in the light–dark box and open-field arena: role of equipment and procedure. Physiol. Behav 30–38.

Lad HV, Liu L, Paya-Cano JL, Parsons MJ, Kember R, Fernandes C, Schalkwyk LC, 2010. Behavioural battery testing: evaluation and behavioural outcomes in 8 inbred mouse strains. Physiol. Behav 99, 301–316. [PubMed: 19931548]

Lein ES, Hawrylycz MJ, Ao N, Ayres M, Bensinger A, Bernard A, Boe AF, Boguski MS, Brockway KS, Byrnes EJ, et al. , 2007. Genome-wide atlas of gene expression in the adult mouse brain. Nature 445, 168–176. [PubMed: 17151600]

Lu T, Aron L, Zullo J, Pan Y, Kim H, Chen Y, Yang TH, Kim HM, Drake D, Liu XS, et al. , 2014. REST and stress resistance in ageing and Alzheimer's disease. Nature 507, 448–454. [PubMed: 24670762]

Maenner MJ, Shaw KA, Baio J, Washington A, Patrick M, DiRienzo M, Christensen DL, Wiggins LD, Pettygrove S, Andrews JG, et al. , 2020. Prevalence of autism Spectrum disorder among children aged 8 years — autism and developmental disabilities monitoring network, 11 sites, United States, 2016. MMWR Surveill. Summ 1–12.

Mastrangelo M, Tolve M, Martinelli M, Di Noia SP, Parrini E, Leuzzi V, 2018. PRICKLE1-related early onset epileptic encephalopathy. Am. J. Med. Genet. A 176, 2841–2845. [PubMed: 30345727]

McIlwain KL, Merriweather MY, Yuva-Paylor LA, Paylor R, 2001. The use of behavioral test batteries: effects of training history. Physiol. Behav 73, 705–717. [PubMed: 11566205]

Nelson SB, Valakh V, 2015. Excitatory/inhibitory balance and circuit homeostasis in autism spectrum disorders. Neuron 87, 684–698. [PubMed: 26291155]

Paemka L, Mahajan VB, Skeie JM, Sowers LP, Ehaideb SN, Gonzalez-Alegre P, Sasaoka T, Tao H, Miyagi A, Ueno N, et al. , 2013. PRICKLE1 interaction with SYNAPSIN I reveals a role in autism spectrum disorders. PLoS One 8 e80737. [PubMed: 24312498]

Paylor R, Spencer CM, Yuva-Paylor LA, Pieke-Dahl S, 2006. The use of behavioral test batteries, II: effect of test interval. Physiol. Behav 87, 95–102. [PubMed: 16197969]

Prut L, Belzung C, 2003. The open field as a paradigm to measure the effects of drugs on anxiety-like behaviors: a review. Eur. J. Pharmacol 463, 3–33. [PubMed: 12600700]

Russ SA, Larson K, Halfon N, 2012. A national profile of childhood epilepsy and seizure disorder. Pediatrics 129, 256–264. [PubMed: 22271699]

Shimojo M, Hersh LB, 2003. REST/NRSF-interacting LIM domain protein, a putative nuclear translocation receptor. Mol. Cell. Biol 23, 9025–9031. [PubMed: 14645515]

Shimojo M, Hersh LB, 2006. Characterization of the REST/NRSF-interacting LIM domain protein (RILP): localization and interaction with REST/NRSF. J. Neurochem 96, 1130–1138. [PubMed: 16417580]

Sowers LP, Loo L, Wu Y, Campbell E, Ulrich JD, Wu S, Paemka L, Wassink T, Meyer K, Bing X, et al. , 2013. Disruption of the non-canonical Wnt gene PRICKLE2 leads to autism-like behaviors with evidence for hippocampal synaptic dysfunction. Mol. Psychiatry 18, 1077–1089. [PubMed: 23711981]

Sweede M, Ankem G, Chutvirasakul B, Azurmendi HF, Chbeir S, Watkins J, Helm RF, Finkielstein CV, Capelluto DG, 2008. Structural and membrane binding properties of the prickle PET domain. Biochemistry 47, 13524–13536. [PubMed: 19053268]

Tao H, Manak JR, Sowers L, Mei X, Kiyonari H, Abe T, Dahdaleh NS, Yang T, Wu S, Chen S, et al. , 2011. Mutations in prickle orthologs cause seizures in flies, mice, and humans. Am. J. Hum. Genet 88, 138–149. [PubMed: 21276947]

Thakar S, Wang L, Yu T, Ye M, Onishi K, Scott J, Qi J, Fernandes C, Han X, Yates JR, et al. , 2017. Evidence for opposing roles of Celsr3 and Vangl2 in glutamatergic synapse formation. Proc. Natl. Acad. Sci. U. S. A 114, E610–E618. [PubMed: 28057866]

Todd BP, Bassuk AG, 2018. A de novo mutation in PRICKLE1 associated with myoclonic epilepsy and autism spectrum disorder. J. Neurogenet 32, 313–315. [PubMed: 29790814]

Tree DR, Shulman JM, Rousset R, Scott MP, Gubb D, Axelrod JD, 2002. Prickle mediates feedback amplification to generate asymmetric planar cell polarity signaling. Cell 109, 371–381. [PubMed: 12015986]

Walf AA, Frye CA, 2007. The use of the elevated plus maze as an assay of anxiety-related behavior in rodents. Nat. Protoc 2.2, 322–328. [PubMed: 17406592]

Zou Y, 2020. Breaking symmetry - cell polarity signaling pathways in growth cone guidance and synapse formation. Curr. Opin. Neurobiol 63, 77–86. [PubMed: 32361599]

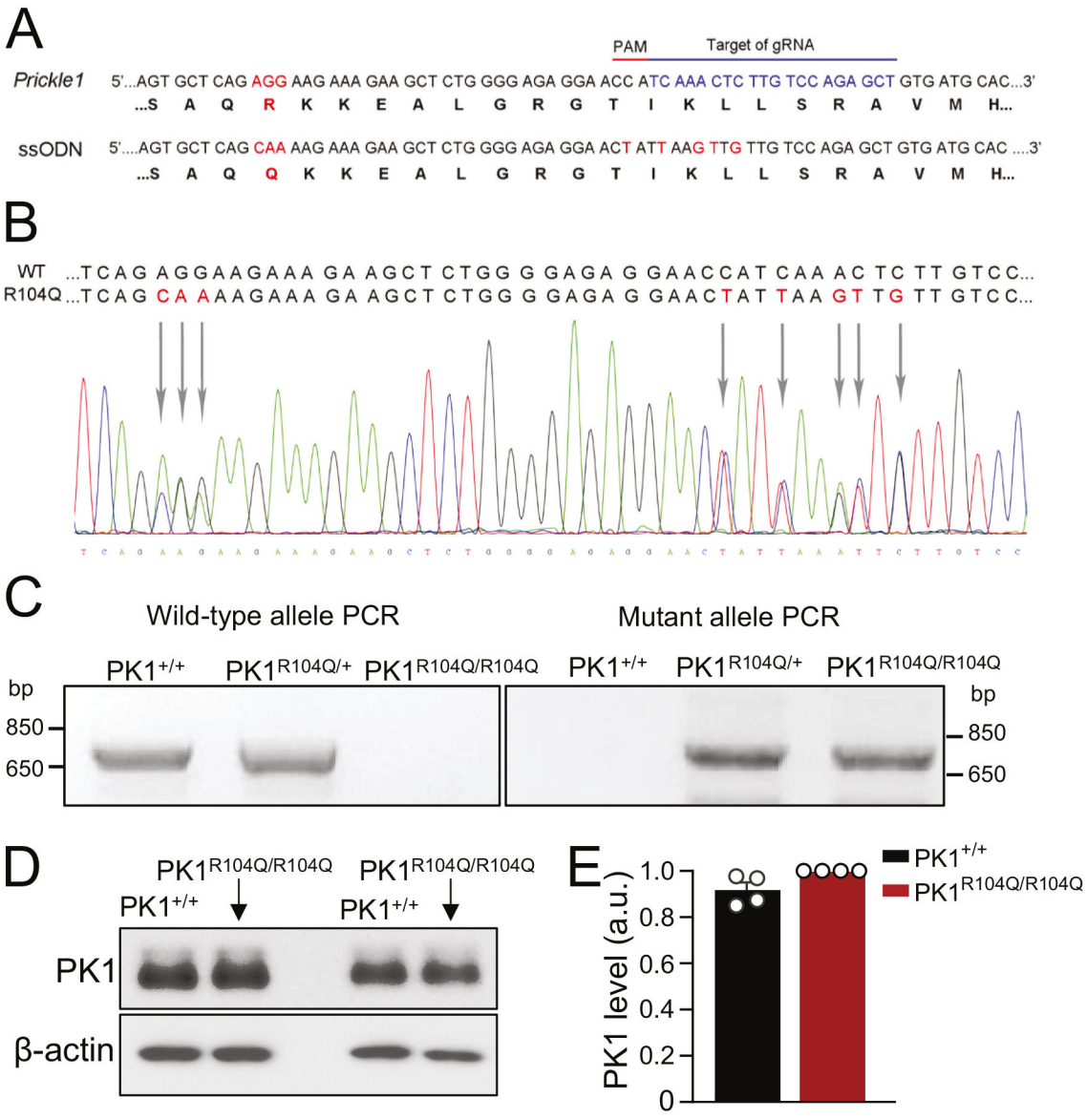

Fig. 1.

Generation of *PK1 R104Q* mice using CRISPR-Cas9-mediated gene editing. (**A**) Top: the original nucleotide sequence of mouse *PK1*, and its corresponding guide RNA target site and protospacer adjacent motif (PAM) sequence. Bottom: sequence of ssODN. Residues 310–312 AGG were replaced by CAA in order to generate Arginine (R) to Glutamine (Q) mutation at position 104. Additional synonymous mutations were generated to prevent Cas9 protein from cleaving the target site after homology-directed repair. (**B**) Sequence analysis of a representative $PK1^{R104Q/+}$ mouse carrying the mutant allele as well as a *WT* allele. (**C**) The CRISPR-targeted *PK1* locus was PCR amplified from genomic tail DNA of $PK1^{+/+}$, $PK1^{R104Q/+}$, and $PK1^{R104Q/R104Q}$ mice and PCR products were size-separated by electrophoresis on a 2% agarose gel for 40 min. The amplicon size is 717 bp for the *WT* allele and 718 bp for the mutant allele. (**D, E**) Western blot analysis of the level of PK1 in

the synaptosome fraction from the cortex and HPC of P14 mice ($PK1^{+/+}$: $n = 4$ animals, $PK1^{R104Q/R104Q}$: $n = 4$ animals). β-actin controls for loading.

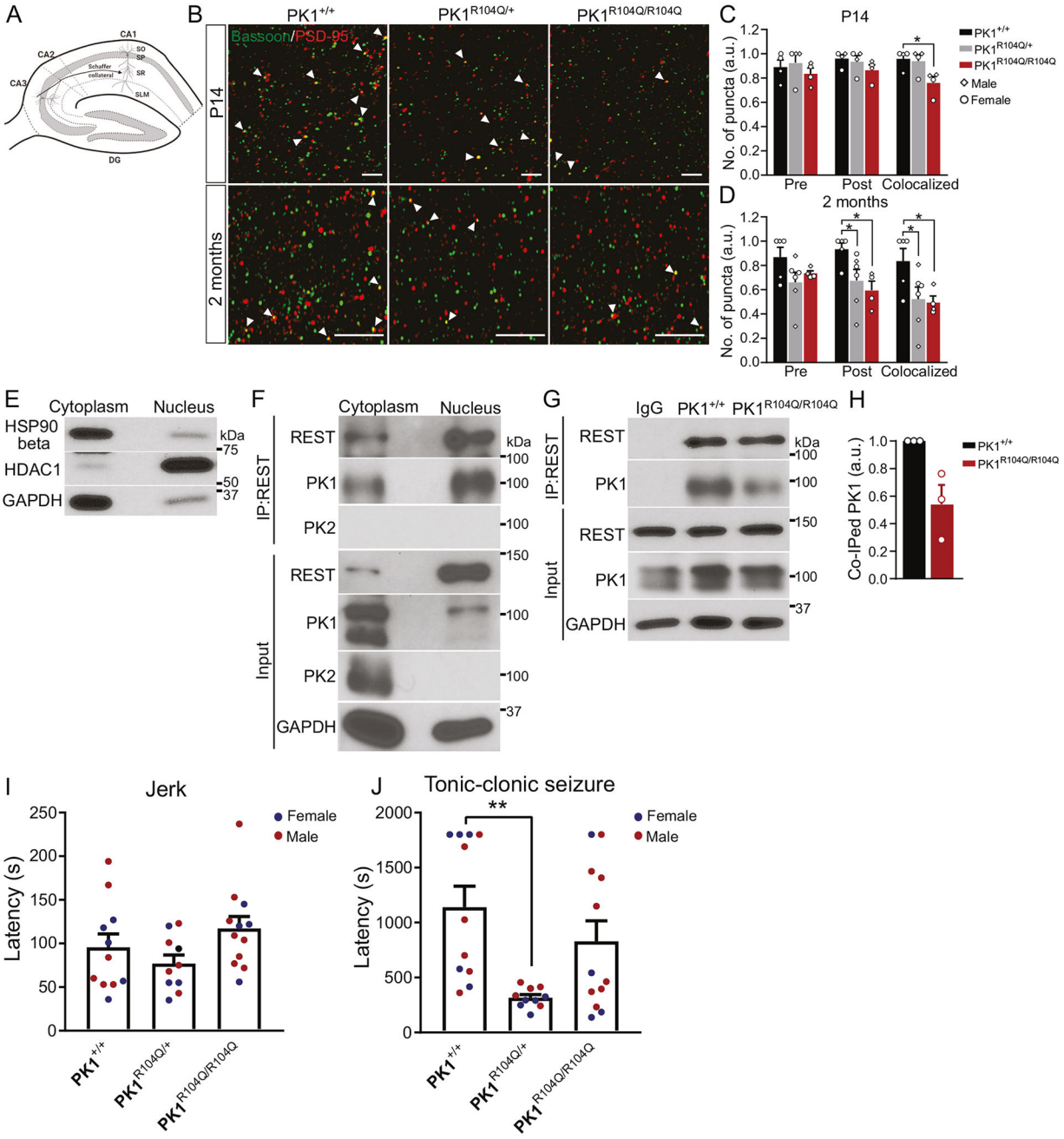

Fig. 2.

The *PK1 R104Q* mice have reduced excitatory synapse numbers, impaired interaction with REST and decreased seizure threshold. (**A**) Schematic diagram of the structure of the mouse HPC. DG, dentate gyrus; SO, stratum oriens; SP, stratum pyramidale; SR, stratum radiatum; SLM, statum lacunosum moleculare. (**B**) Immunostaining for pre- (green; Bassoon) and postsynaptic puncta (red; PSD-95) of glutamatergic synapses in hippocampal CA1 SR from P14 and adult $PK1^{+/+}$, $PK1^{R104Q/+}$ and $PK1^{R104Q/R104Q}$ mice. Arrow heads indicate colocalized puncta. (**C,D**) Quantification of the number of pre-, postsynaptic puncta as well as glutamatergic synapses identified by colocalized puncta. Each data point represents

the average number of puncta calculated from images taken within one animal. One-way ANOVA, * $p < 0.05$. (**E**) Western blot analysis of cytoplasmic protein (HSP90 beta) and nuclear protein (HDAC1) to indicate the efficiency of the separation of cytoplasmic and nuclear fraction of mouse HPC. $PK1^{+/+}$: $n = 3$ animals, $PK1^{R104Q/R104Q}$: $n = 3$ animals. Three independent experiments showed consistent results. (**F**) IP assay was performed to test the interaction between REST and PK1 using the cytoplasmic and nuclear lysate of HPC from adult *WT* mice. (**G, H**) CoIP to test the interaction between REST and PK1. (**I**)The latency to the first observation of jerk was measured following 50 mg/kg PTZ administration. $PK1^{+/+}$: $n = 11$ (5♀, 6♂), $PK1^{R104Q/+}$: $n = 10$ (5♀, 5♂), $PK1^{R104Q/R104Q}$: $n = 12$ (4♀, 7♂). One-way ANOVA, DF = 32, $F(2,30) = 2.219$, $p = 0.1263$. (**J**) The latency to the onset of tonic-clonic seizure. $PK1^{+/+}$: $n = 11$ (5♀, 6♂), $PK1^{R104Q/+}$: $n = 10$ (5♀, 5♂), $PK1^{R104Q/R104Q}$: $n = 12$ (4♀, 7♂). One-way ANOVA, DF = 32, $F(2, 30) = 2.219$, $p = 0.1263$. One-way ANOVA, DF = 32, $F(2, 30) = 6.195$, $p = 0.0056$. Turkey's multiple comparisons test revealed a significant difference between $PK1^{+/+}$ and $PK1^{R104Q/+}$ group ($p = 0.0042$). Results are means ± SEM.

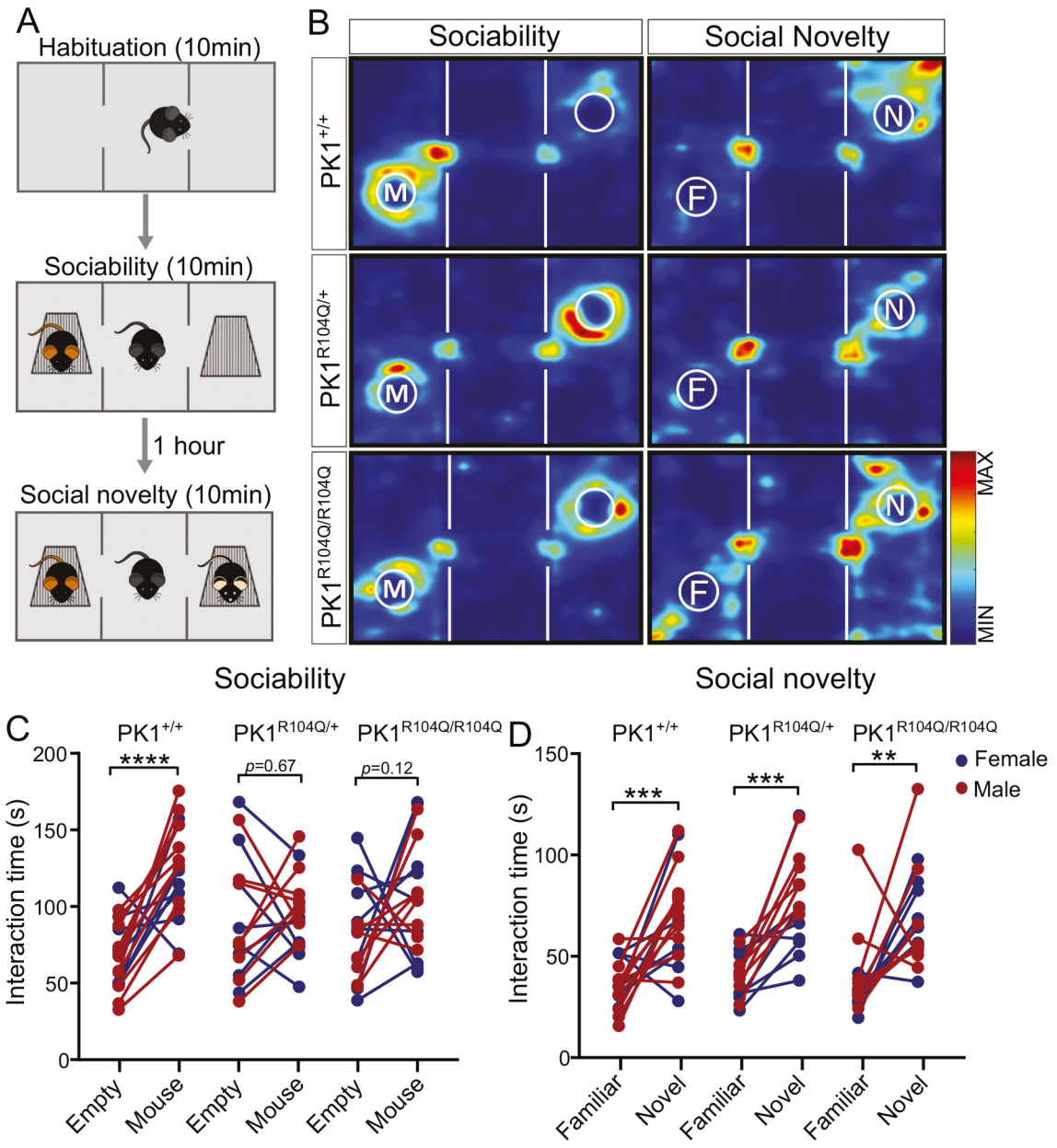

Fig. 3.

The *PK1 R104Q* mice display impaired social interaction but normal social memory in three-chamber social interaction test. (**A**) Schematic of the three-chamber social interaction test. (**B**) Representative heatmap images showing the track of animal's snout in the three-chamber social interaction apparatus. Red represents increased time spent and blue represents minimal time spent during trial. "M" in white circle represents the location of non-littermate stranger mouse restrained under a steel wire pencil cup. White circle without fill indicates empty pencil cup. F: familiar mouse, N: novel mouse. (**C**) Scatter plot shows the time mice spent sniffing the stranger mouse versus the empty cup during the social approach test. $PK1^{+/+}$: n = 18 (7♀, 11♂), $PK1^{R104Q/+}$: n = 16 (8♀, 8♂), $PK1^{R104Q/R104Q}$: n = 17 (9♀, 8♂). (**D**) Scatter plot shows the time spent sniffing the novel mouse versus the

familiar mouse during the social memory test. $PK1^{+/+}$: $n = 18$ (7♀, 11♂), $PK1^{R104Q/+}$: $n = 15$ (8♀, 7♂), $PK1^{R104Q/R104Q}$: $n = 17$ (9♀, 8♂). Paired t-test, ** $p < 0.01$, *** $p < 0.001$, **** $p < 0.0001$.

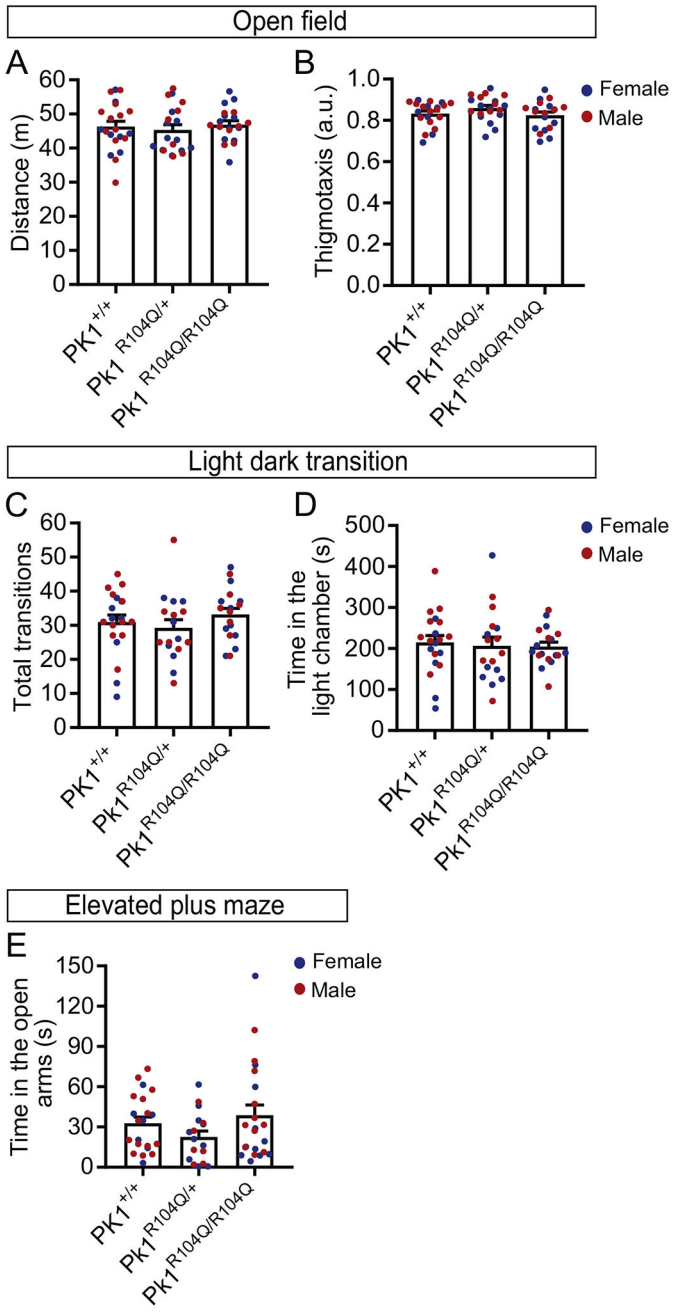

Fig. 4.

The *PK1 R104Q* mice have normal locomotor activity and anxiety level. (**A**) Animal's general locomotor activity in the OFA was evaluated by the measurement of total distance traveled during the 10-min test period. $PK1^{+/+}$: $n = 21$ (8♀, 13♂), $PK1^{R104Q/+}$: $n = 20$ (11♀, 9♂), $PK1^{R104Q/R104Q}$: $n = 20$ (11♀, 9♂). One-way ANOVA, DF = 60, $F(2, 58) = 0.3007$, $p = 0.7415$. (**B**) Thigmotaxis (a tendency to remain close to the vertical wall) was calculated as the proportion of time animals stay in the border zone. The OFA is 40 × 40 × 34 cm^3 which was divided into a 20 cm × 20 cm central zone and the surrounding border zone for video analysis. $PK1^{+/+}$: $n = 21$, $PK1^{R104Q/+}$: $n = 20$, $PK1^{R104Q/R104Q}$: $n = 20$. One-way ANOVA,

DF = 60, $F(2, 58) = 1.645$, $p = 0.2019$. (**C**) Number of transitions between the light and dark compartments in the LDT test was measured to assess animal's locomotor activity. $PK1^{+/+}$: $n = 20$ (8♀, 12♂), $PK1^{R104Q/+}$: $n = 17$ (8♀, 9♂), $PK1^{R104Q/R104Q}$: $n = 18$ (10♀, 8♂). One-way ANOVA, DF = 54, $F(2, 52) = 0.8304$, $p = 0.4416$. (**D**) Time spent in the light chamber was measured to evaluate anxiety level. Shorter time in the light chamber suggest higher anxiety level. $PK1^{+/+}$: $n = 20$, $PK1^{R104Q/+}$: $n = 17$, $PK1^{R104Q/R104Q}$: $n = 18$. One-way ANOVA, DF = 54, $F(2, 52) = 0.1053$, $p = 0.9002$. (**E**) Animal's anxiety level was evaluated by the time spent in the open arms of the EPM. $PK1^{+/+}$: $n = 21$ (7♀, 14♂), $PK1^{R104Q/+}$: $n = 17$ (10♀, 7♂), $PK1^{R104Q/R104Q}$: $n = 22$ (11♀, 11♂). One-way ANOVA, DF = 59, $F(2, 57) = 1.708$, $p = 0.1903$. Results are means ± SEM.

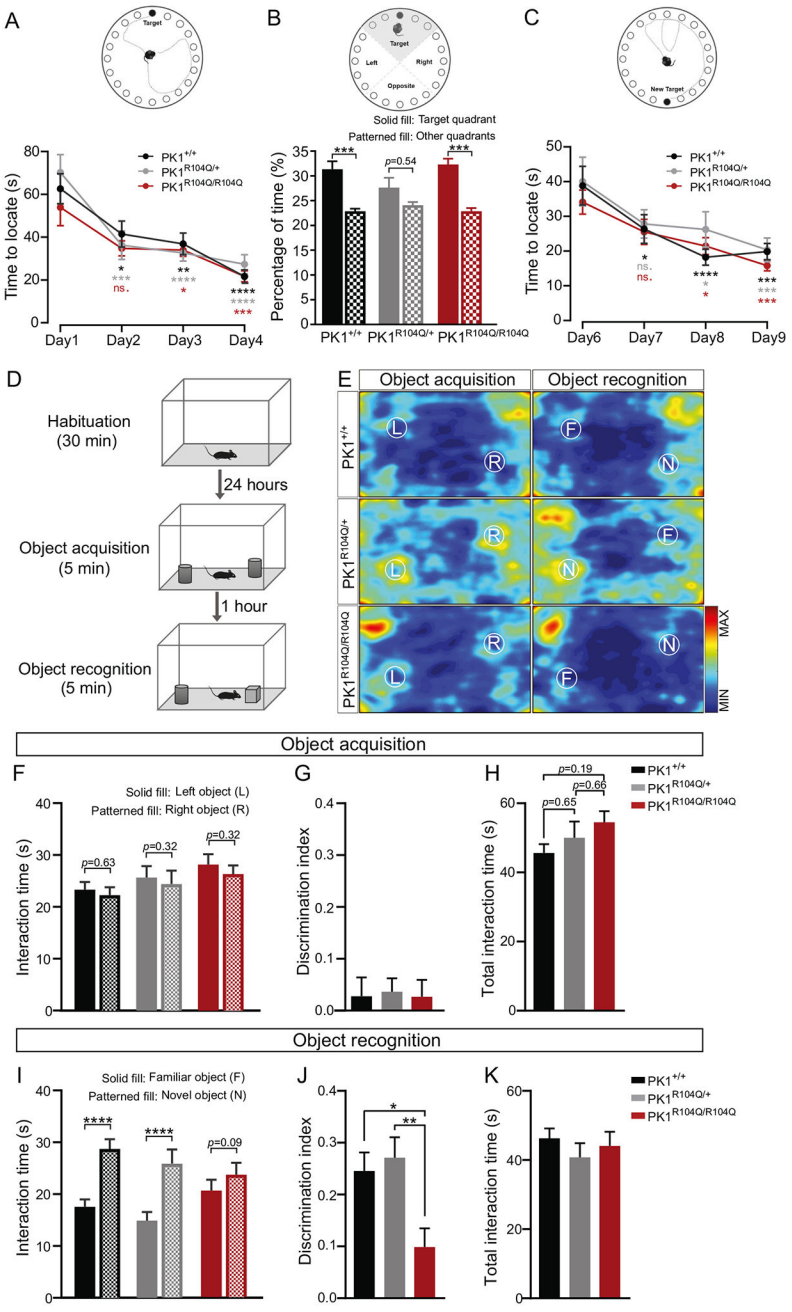

Fig. 5.

Mild spatial memory deficit and impaired object recognition in the *PK1 R104Q* mice. (**A**) The latency to locate the real escape hole of each animal was measured during the acquisition training phase (day1-day4). $PK1^{+/+}$: $n = 21$(8♀, 13♂), $PK1^{R104Q/+}$: $n = 17$ (8♀, 9♂), $PK1^{R104Q/R104Q}$: $n = 19$ (10♀, 9♂). Two-way repeated-measures ANOVA: genotype × time $F(6, 162) = 0.6545$, $p = 0.6865$; time $F(3, 162) = 27.37$, $p < 0.0001$; genotype $F(2, 54) = 0.9518$, $p = 0.3924$. Tukey's multiple comparisons test, $PK1^{+/+}$: Day1 vs. Day2 $p = 0.0204$, Day1 vs. Day3 $p = 0.0028$, Day1 vs. Day4 $p < 0.0001$; $PK1^{R104Q/+}$: Day1 vs. Day2 $p = 0.0002$, Day1 vs. Day3 $p < 0.0001$, Day1 vs. Day4 $p < 0.0001$; $Pk1^{R104Q/R104Q}$:

Day1 vs. Day2 $p = 0.0617$, Day1 vs. Day3 $p = 0.0475$, Day1 vs. Day4 $p < 0.0002$. (**B**) During the probe test, the maze was divided into four quadrants (target, opposite, left and right). Each quadrant contains five escape holes. The real escape hole was located in the center of the target quadrant. Bar graph shows the time animals spent in the target quadrant versus the average time animals spent in the other three quadrants. $PK1^{+/+}$: $n = 21$(8♀, 13♂), $PK1^{R104Q/+}$: $n = 17$ (8♀, 9♂), $PK1^{R104Q/R104Q}$: $n = 19$ (10♀, 9♂). Wilcoxon matched-pairs signed rank test, $PK1^{+/+}$ $p = 0.0004$;$PK1^{R104Q/+}$ $p = 0.5477$; $PK1^{R104Q/R104Q}$ $p = 0.0003$. (**C**) The latency to locate the new real escape hole was measured during the reversal training (day6-day9). $PK1^{+/+}$: $n = 19$(7♀, 12♂), $PK1^{R104Q/+}$: $n = 16$(7♀, 9♂), $PK1^{R104Q/R104Q}$: $n = 17$(9♀, 8♂). Two-way repeated-measures ANOVA: genotype × time $F(6, 147) = 0.85$, $p = 0.6865$; time $F(3, 147) = 18.88$, $p < 0.0001$; genotype $F(2, 49) = 0.6037$, $p = 0.5508$. Tukey's multiple comparisons test, $PK1^{+/+}$: Day6 vs. Day7 $p = 0.0294$, Day6 vs. Day8 $p < 0.0001$, Day6 vs. Day9 $p = 0.0002$; $PK1^{R104Q/+}$: Day6 vs. Day7 $p = 0.0611$, Day6 vs. Day8 $p = 0.0259$, Day6 vs. Day9 $p = 0.0005$; $Pk1^{R104Q/R104Q}$: Day6 vs. Day7 $p = 0.2661$, Day6 vs. Day8 $p = 0.0395$, Day6 vs. Day9 $p = 0.0009$. (**D**) Schematic of the novel object recognition test. (**E**) representative heatmap images showing the location of animal's snout in the novel object recognition task. Red represents increased time spent and blue represents minimal time spent during trial. L: left object, R: right object, F: familiar object, N: novel object. (**F-I**) Animal's performance during the acquisition training phase. $PK1^{+/+}$: $n = 16$ (5♀, 11♂), $PK1^{R104Q/+}$: $n = 16$ (7♀, 9♂), $PK1^{R104Q/R104Q}$: $n = 16$ (7♀, 9♂). (**F**) Bar graphs show the time mice spent sniffing the left object (T_L) versus the right object (T_R). Wilcoxon matched-pairs signed rank test, $PK1^{+/+}$ $p = 0.6322$, $PK1^{R104Q/+}$ $p = 0.3225$, $PK1^{R104Q/R104Q}$ $p = 0.3162$. (**G**) The discrimination index $(T_L\text{-}T_R)/(T_L + T_R)$. One-way ANOVA, DF = 47, $F(2, 45) = 0.02735$, $p = 0.973$. (**H**)The total time animals spent sniffing both objects. One-way ANOVA, DF = 47, $F(2, 45) = 1.538$, $p = 0.2259$. (**I-K**) Animal's performance during the object recognition phase. $PK1^{+/+}$: $n = 16$ (5♀, 11♂), $PK1^{R104Q/+}$: $n = 16$ (7♀, 9♂), $PK1^{R104Q/R104Q}$: $n = 16$ (7♀, 9♂). (**I**)Bar graphs show the time mice spent sniffing the familiar object (T_F)versus the novel object (T_N). Wilcoxon matched-pairs signed rank test, $PK1^{+/+}$ $p < 0.0001$, $PK1^{R104Q/+}$ $p < 0.0001$, $PK1^{R104Q/R104Q}$ $p = 0.0916$. (**J**) The discrimination index $(T_N - T_F)/(T_N + T_F)$. One-way ANOVA, DF = 47, $F(2, 45) = 6.272$, $p = 0.004$. Tukey's multiple comparisons test, * $p < 0.05$, ** $p < 0.01$. (**K**) The total time animals spent interacting with both objects. One-way ANOVA, DF = 47, $F(2, 45) = 0.5523$, $p = 0.5795$. Results are means ± SEM.